

# Neurophotonics

Neurophotonics.SPIEDigitalLibrary.org

## **Functional near-infrared spectroscopy for speech protocols: characterization of motion artifacts and guidelines for improving data analysis**

Sergio L. Novi  
Erin Roberts  
Danielle Spagnuolo  
Brianna M. Spilsbury  
D'manda C. Price  
Cara A. Imbalzano  
Edwin Forero  
Arjun G. Yodh  
Glen M. Tellis  
Cari M. Tellis  
Rickson C. Mesquita

Sergio L. Novi, Erin Roberts, Danielle Spagnuolo, Brianna M. Spilsbury, D'manda C. Price, Cara A. Imbalzano, Edwin Forero, Arjun G. Yodh, Glen M. Tellis, Cari M. Tellis, Rickson C. Mesquita, "Functional near-infrared spectroscopy for speech protocols: characterization of motion artifacts and guidelines for improving data analysis," *Neurophoton.* **7**(1), 015001 (2020), doi: 10.1117/1.NPh.7.1.015001

**SPIE.**

# Functional near-infrared spectroscopy for speech protocols: characterization of motion artifacts and guidelines for improving data analysis

Sergio L. Novi,<sup>a,b</sup> Erin Roberts,<sup>c</sup> Danielle Spagnuolo,<sup>c</sup>  
Brianna M. Spilsbury,<sup>c</sup> D'manda C. Price,<sup>c</sup> Cara A. Imbalzano,<sup>c</sup>  
Edwin Forero,<sup>a,b</sup> Arjun G. Yodh,<sup>d</sup> Glen M. Tellis,<sup>c</sup> Cari M. Tellis,<sup>c</sup>  
and Rickson C. Mesquita<sup>a,b,\*</sup>

<sup>a</sup>University of Campinas, Institute of Physics, Campinas, São Paulo, Brazil

<sup>b</sup>Brazilian Institute of Neuroscience and Neurotechnology, Campinas, São Paulo, Brazil

<sup>c</sup>Misericordia University, Department of Speech-Language Pathology, Dallas, Pennsylvania, United States

<sup>d</sup>University of Pennsylvania, Department of Physics and Astronomy, Philadelphia, Pennsylvania, United States

**Abstract.** Monitoring speech tasks with functional near-infrared spectroscopy (fNIRS) enables investigation of speech production mechanisms and informs treatment strategies for speech-related disorders such as stuttering. Unfortunately, due to movement of the temporalis muscle, speech production can induce relative movement between probe optodes and skin. These movements generate motion artifacts during speech tasks. In practice, spurious hemodynamic responses in functional activation signals arise from lack of information about the consequences of speech-related motion artifacts, as well as from lack of standardized processing procedures for fNIRS signals during speech tasks. To this end, we characterize the effects of speech production on fNIRS signals, and we introduce a systematic analysis to ameliorate motion artifacts. The study measured 50 healthy subjects performing jaw movement (JM) tasks and found that JM produces two different patterns of motion artifacts in fNIRS. To remove these unwanted contributions, we validate a hybrid motion-correction algorithm based sequentially on spline interpolation and then wavelet filtering. We compared performance of the hybrid algorithm with standard algorithms based on spline interpolation only and wavelet decomposition only. The hybrid algorithm corrected 94% of the artifacts produced by JM, and it did not lead to spurious responses in the data. We also validated the hybrid algorithm during a reading task performed under two different conditions: reading aloud and reading silently. For both conditions, we observed significant cortical activation in brain regions related to reading. Moreover, when comparing the two conditions, good agreement of spatial and temporal activation patterns was found only when data were analyzed using the hybrid approach. Overall, the study demonstrates a standardized processing scheme for fNIRS data during speech protocols. The scheme decreases spurious responses and intersubject variability due to motion artifacts. © The Authors. Published by SPIE under a Creative Commons Attribution 4.0 Unported License. Distribution or reproduction of this work in whole or in part requires full attribution of the original publication, including its DOI. [DOI: [10.1117/1.NPh.7.1.015001](https://doi.org/10.1117/1.NPh.7.1.015001)]

**Keywords:** functional near-infrared spectroscopy; motion artifacts; speech protocols; jaw movement; temporal muscle; reading protocols.

Paper 19082R received Aug. 27, 2019; accepted for publication Dec. 19, 2019; published online Jan. 10, 2020.

## 1 Introduction

Functional near-infrared spectroscopy (fNIRS) is a robust tool for measuring brain function.<sup>1-8</sup> It probes the brain using the differential absorption of near-infrared (NIR) light by hemoglobin. Owing to features such as high temporal resolution, low cost, and portability, fNIRS is frequently

---

\*Address all correspondence to: Rickson C. Mesquita, E-mail: [rickson@ifi.unicamp.br](mailto:rickson@ifi.unicamp.br)

chosen by researchers to investigate human populations ranging from neonates<sup>9–24</sup> to patients with severe injuries.<sup>2,25,26–31</sup> Moreover, fNIRS is useful during a variety of activities, even in unconstrained environments.<sup>32–34</sup> In speech task applications, for example, fNIRS can potentially determine whether cerebral blood oxygenation changes in subjects with speech and language disabilities are different from those of normal subjects,<sup>8,35–37</sup> and fNIRS could track motor learning during treatment of individuals with voice disorders.

Several advances in preprocessing of fNIRS data are needed to bring speech applications to fruition. One important fNIRS limitation concerns the contribution of extracortical layers to the fNIRS signal. Light interacts with superficial layers such as the scalp, in addition to the cortex. Thus, hemodynamic changes in superficial layers and/or global systemic changes in the brain can affect fNIRS measurements and can produce misleading results and interpretation.<sup>38–45</sup> One approach to address this problem, which has been partially successful, is to add detectors close to the light sources (typically source–detector separations less than 1 cm). These source–detector pairs are predominantly sensitive to the layers above the cortex, and one can use their information to account for extracortical signal contributions.<sup>40,46</sup> In speech protocols, for example, it is known that partial pressure of arterial CO<sub>2</sub> (PaCO<sub>2</sub>) varies during inner and outer speech tasks,<sup>47–49</sup> and the data in the short-separation channels can help remove systemic physiological contributions that are simultaneously present in both extracortical and cortical tissues.<sup>46</sup>

Another confounding factor is the motion artifact, which can produce misleading hemodynamic data based on spurious fNIRS responses.<sup>50</sup> Motion artifacts largely originate from relative movement between the subject's head and the optodes and are generally characterized as spikes and/or baseline changes in the recorded light intensity.<sup>51–53</sup> Several methods to correct the fNIRS signals for motion artifacts have been proposed.<sup>51,54,55</sup> However, the fNIRS community still lacks the “standard,” general guidelines for properly removing motion artifacts from measurements.<sup>53</sup> Progress is needed because motion artifacts can produce misleading results and conclusions.

The problem of motion artifacts is particularly critical for tasks involving speech, since the movement of the jaw is inherent to speech production and dramatically affects coupling between optodes and the scalp. During speech, the temporalis muscle is responsible for moving the jaw. It contracts and relaxes, moving from its resting position and producing motion artifacts in fNIRS data. These artifacts have been previously reported,<sup>53,56,57</sup> but the processes by which they affect fNIRS signals are not fully understood. Jaw movement (JM) artifacts, in particular, represent the main application limitation for fNIRS investigations of the mechanisms underlying speech. The creation of a standard, well-validated, and robust method for correcting speech-related processing protocols will facilitate better investigation of speech production, improved understanding of brain mechanisms associated with communication disorders, and validation of treatment strategies for speech disorders.

In this work, we investigate the fNIRS responses in speech-related tasks. We hypothesize that jaw motion produces motion artifacts generated by tasks involving speech production, and we use the JM (only) task to characterize the effect that motion artifacts have on fNIRS signals during speech tasks. This protocol enabled us to validate a hybrid motion artifact algorithm for removing unwanted artifacts related to JM in speech during fNIRS measurements. The efficacy of the proposed algorithm was tested in reading tasks performed by 41 healthy subjects. In these studies, we compared subject fNIRS responses while reading aloud with the fNIRS responses in the same subjects when reading silently. We found no significant difference in both reading tasks “after” application of the correction procedure. Overall, the results demonstrate that the new correction algorithm can efficiently remove motion artifacts due to speech. This advance, in turn, should open new opportunities for fNIRS in functional protocols involving speech.

## 2 Materials and Methods

### 2.1 Subjects and Experimental Protocol

We acquired data from 52 healthy young volunteers (26 females) with ages ranging from 18 to 23 years [mean (standard deviation) = 20 years old (3)]. Data from one subject were discarded due to bad optical coupling in most of the locations measured. Of the remaining volunteers,

41 subjects (20 females) performed randomized block-designed paradigms with 10 repetitions of three distinct tasks: JM, reading aloud (RA), and silent reading (SR).

For the JM task, we instructed each subject to simply move their jaws for a period of 5 s followed by 5 s of rest. With this task, we aimed to isolate artifacts caused by JM during speech production. To further elucidate the impact of longer periods of JM in fNIRS recordings, a sub-cohort of 10 subjects (six females) performed the JM task for a period of 10 s followed by 20 s of rest. In the RA and the SR tasks, each subject read a small passage aloud and silently, respectively, for 10 s followed by 10 s of rest. The reading text was standardized at a third- or fourth-grade reading level. Thus, the subjects were not cognitively challenged. All instructions were presented on a computer screen, and the experimental protocol took  $\sim 19$  min. The experimental protocol was approved by the local ethical committee and was conducted in accordance with the Misericordia University Institutional Review Board policies, where the measurements were carried out, following the principles from Helsinki II Convention from 20 August 1947. All subjects provided written informed consent prior to data acquisition.

## 2.2 Functional Near-Infrared Spectroscopy Signal Acquisition

We acquired all fNIRS data with a commercial continuous-wave NIRS system (NIRScout, NIRx Medical Systems, New York). The optical probe contained 16 sources at two different wavelengths (LEDs centered at 760 and 850 nm,  $\sim 15$  mW light power emission for each) and 16 detectors. This configuration enabled the use of 32 source–detector combinations (i.e., channels) at 3 cm, and two source–detector pairs at 0.8 cm (short channels). Data were acquired at 7.8 Hz.

The probe design was arranged to be sensitive to the primary regions related to language and speech in the frontal, temporal, and parietal lobes. We positioned one short channel in each brain hemisphere. The short-channel data enabled us to regress out extracortical contributions hemispherically. To secure the optodes on the heads of the subjects, we used a 10–20 standard cap from NIRx Medical Systems.<sup>58</sup> We digitized the position of all optodes using a commercial digitizer (Fastrack, Polhemus, Colchester, Vermont) for better accuracy concerning the location of each source and detector. Figure 1(a) shows a sensitive profile for the probe, which was obtained from Monte Carlo simulations through the AtlasViewer package.<sup>59</sup>

## 2.3 Functional Near-Infrared Spectroscopy Data Analysis

To estimate hemoglobin concentration changes from fNIRS data, we wrote homemade scripts based on existing HomER 2 functions.<sup>50</sup> The processing workflow is depicted in Fig. 1(b). First, we discarded channels with low signal-to-noise ratio (SNR) from the analysis. SNR was computed as the mean intensity of each channel divided by the standard deviation of the same

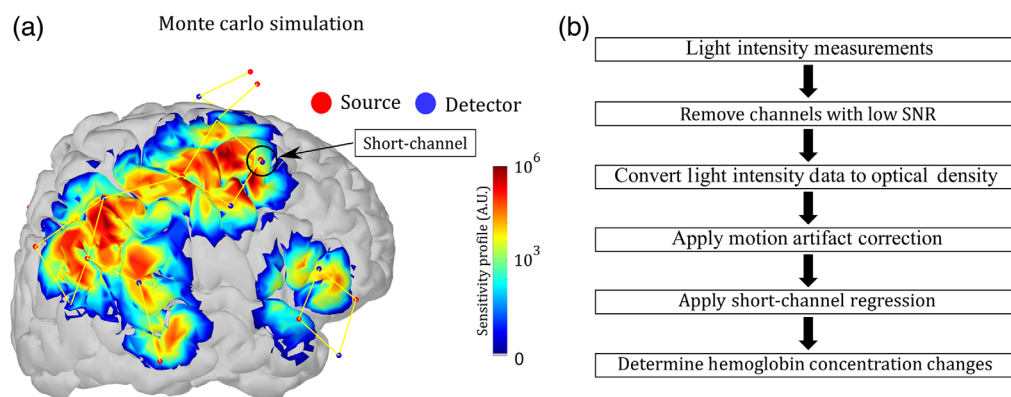


**Fig. 1** (a) Sensitivity profile of the optical probe on the right hemisphere. The probe was designed to cover most of the cortical regions related to speech, and it has a hemispherical symmetry. It employs 32 long-channels with source–detector separation of 3 cm, and two short-channels with source–detector separation of 0.8 cm. The short-channels were located in the frontal lobe (indicated in the figure). (b) Workflow of the preprocessing steps of fNIRS data.

channel. Our previous experience with fNIRS data found that channels with SNR  $<8$  are very noisy and do not contain useful information.<sup>12,13,30</sup> On the other hand, thresholds set higher than 8 sometimes discard good channels (i.e., channels that contain useful information).

Next, we converted light intensity from the remaining channels into optical density. Since we sought to understand the effects of motion at any frequency on the optical signal, we opted not to band-pass filter temporal fluctuations of the data for analysis. We then performed motion artifact correction using the optical density time series (see Sec. 2.4 about this motion artifact correction). After the motion artifact correction, we regressed out the extracortical contributions from superficial layers. Since superficial hemodynamics may not be homogeneously distributed along the scalp,<sup>60</sup> the extracortical data were obtained from the short source–detector channel that was closest to a long separation channel of interest. This scheme minimized the effects of superficial hemodynamics. The regression procedure is described elsewhere.<sup>40,42,44,46</sup> Hemoglobin concentration changes were calculated using the modified Beer–Lambert law with a differential path-length factor of 6 for both wavelengths.<sup>61,62</sup>

For each channel in a single subject, we classified channels that presented typical hemodynamic responses due to neural activity using a general linear model with an adaptive hemodynamic function.<sup>63</sup> The typical response was an increase in oxyhemoglobin and decrease in deoxyhemoglobin concentration synchronized with the period of stimulation. Channels that exhibited significant responses ( $p < 0.05$ ) for oxyhemoglobin and deoxyhemoglobin were considered to be activated during the task.<sup>64–66</sup> To analyze the hemodynamic response function (HRF) of an activated channel, we block-averaged all trials of that channel.

## 2.4 Motion Artifact Correction

Current motion artifact correction algorithms can be classified into two main classes. The first class relies on first identifying time-series points that are contaminated by motion. These algorithms attempt to correct only the contaminated time points. The spline interpolation is probably the most well-known algorithm from this class. In this work, we used an automated version of the MARA algorithm for spline interpolation.<sup>51</sup> Briefly, this spline algorithm identifies contaminated data segments by calculating the standard deviation within a sliding window. The segment correction is made by replacing the original data points with the residue of the data and a cubic spline interpolation. Baseline shifts were corrected by comparing the mean values of the data taken before and after the contaminated segment. More details regarding the spline interpolation algorithm can be found in Sec. S1 in the [Supplementary Material](#).

The second class of algorithm includes those that correct the whole time series based on reliable features from the fNIRS data. Principal component analysis and wavelet decomposition are examples of algorithms that belong to this second class.<sup>55,67</sup> In this work, we employed the wavelet decomposition analysis to correct the motion artifacts, since this algorithm has been used extensively already to process fNIRS data.<sup>53</sup> In wavelet decomposition analysis, each fNIRS time series is decomposed in functions (i.e., wavelets) that are localized in both time and frequency.<sup>55</sup> A correction filter sets wavelet coefficients with values very far outside the central portion of the distribution of coefficients to zero. The reasoning behind this procedure is that outlier coefficients are related to motion. The time series is then reconstructed without motion (see Sec. S2 in the [Supplementary Material](#), for more details about wavelet filtering).

We tested several approaches to perform motion artifact correction. Specifically, we analyzed the efficacy of one algorithm from each class to independently remove speech-related artifacts generated by JM. However, since these algorithms are based on different hypotheses, we further analyzed the effects of a hybrid motion artifact correction algorithm that “sequentially” uses spline and then wavelet decomposition, “in this order.” By employing this hybrid algorithm, we showed that prior spline correction can improve the performance of subsequent wavelet analysis per motion artifact removal.

## 2.5 Statistical Analysis

To extract common activation patterns from the whole group for each task (RA and SR), we performed a full-frequency analysis across all subjects rather than just group averages.

Specifically, channels with (without) the characteristic HRF were assigned with 1 (0) so that we could create binarized classification vectors (BCVs) for each subject. Next, we computed frequency maps for each task by combining all BCVs. Here, we opt to present group results with frequency analysis, because the individual response to functional tasks is very heterogeneous, and thus simple averages do not reflect the whole distribution of responses measured across a group. In addition, the frequency analysis enables one to find the cortical regions that are mostly present in all subjects for a given task, which we have previously shown to be more informative than average property maps; the average property maps are not always representative of individual responses when the distribution of responses is wide across subjects.<sup>12,13,68</sup> Finally, our summaries of the activated patterns related to tasks used three regions of interest (ROIs) known to play a role during reading: Broca's area; Wernicke's area; and the posterior region in the right hemisphere, contralateral to Wernicke's area. The channels in each ROI were manually chosen based on their anatomical position. Owing to lack of accurate spatial information, we averaged the results of the activated channels across all subjects.

### 3 Results

#### 3.1 *Jaw Movement Induces Two Types of Motion Artifacts*

We visually inspected the optical density time series of each channel for each subject during the JM (only) task. We found that movement of the jaw produces strong (apparent) changes at both wavelengths that are temporally correlated with task duration. These changes are easy to be incorrectly assigned as brain activation (i.e., unreal brain activation) in any functional speech task. Concerning location, the changes are broadly distributed over the different regions of the brain related to speech production. Many (a majority of) channels are compromised. Overall, the mean (standard deviation) number of contaminated channels across all subjects was 20 (5), which corresponds to 60% of channels in our optical probe.

The manner in which each channel was affected by JM was not similar. JM primarily induced two types of artifacts in the fNIRS data. The first type (type 1) is characterized by abrupt, non-harmonic oscillations synchronized with the duration of the stimulus [Fig. 2(a)]. The second type of artifact (type 2) introduces baseline changes distributed within the stimulus period. They are similar to motion artifacts commonly found in other functional tasks [Fig. 2(b)]. Type 1 artifacts are present in the short- and long-duration JMs, but artifacts of type 2 become more important as the duration length of the speech task increases. Concerning location, type 1 artifacts mostly affect channels located in the anterior region of the head, i.e., closer to the main parts of the temporalis muscle [Fig. 2(c)]. Type 2 artifacts were most commonly found in posterior channels [Fig. 2(d)]. Some channels, mostly those located between anterior and posterior regions, exhibit both types of artifacts: abrupt oscillations and slower baseline changes.

#### 3.2 *Hybrid Procedure of Wavelet and Spline Removes Artifacts Caused by Jaw Motion*

Since JM is not expected to induce a significant average response variation, the signal mean of the time points immediately before the task should be approximately the same as the mean of the time points during the JM task (note, participants did not read or speak during the JM tasks; they only moved their jaw). However, this effect is not what one observes. We attempted to apply fNIRS motion artifact correction algorithms to remove such artifacts. Across all JM trials for all subjects, wavelet filtering was able to correct ~90% of the trials during the JM task (i.e., corrected data imply that the mean of the time points during the JM task was not significantly different from the mean of the time points immediately before the JM task). The wavelet decomposition could successfully remove abrupt oscillations in the optical density time series, but it did not succeed in correcting the artifacts of type 2. Instead, the wavelet algorithm left/induced long-term trends in intervals of the time series that exhibit baseline changes [Fig. 3(a)].

On the other hand, spline interpolation is very efficient for correcting type 2 artifacts, which are characterized by baseline changes. Spline-only, however, could not remove the abrupt

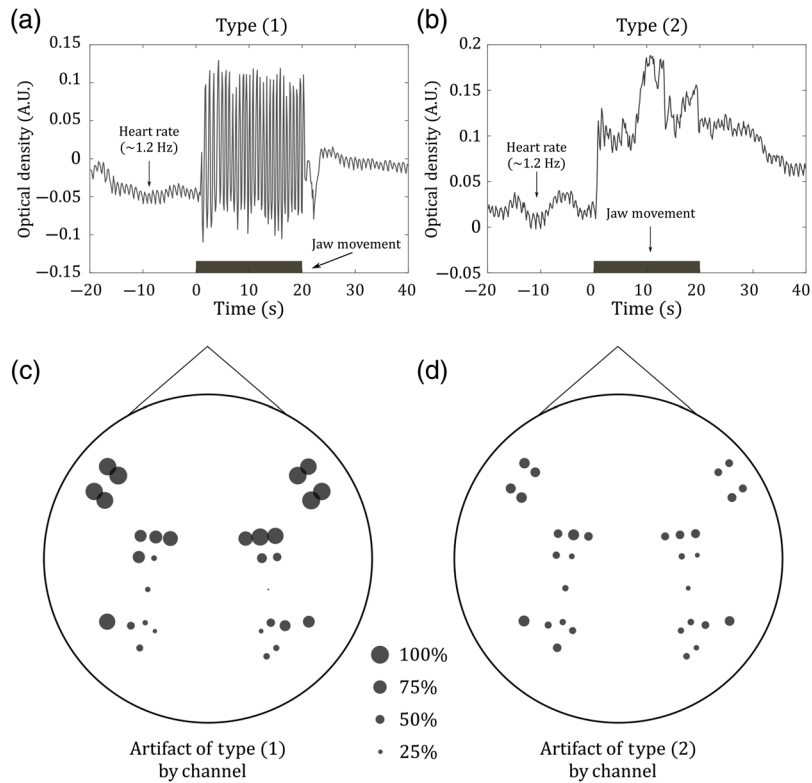


**Fig. 2** Temporal and spatial characterization of motion artifacts due to the movement of the jaw. (a) and (b) Arbitrary data affected by abrupt, nonharmonic oscillations (type 1 artifact) and by a significant change in baseline temporally correlated with the jaw motion (type 2 artifact), respectively. (c) and (d) The spatial distribution of the artifacts of type 1 and type 2, respectively, across all subjects. In the figure, the circles represent the channels, and the size of the circle represents the how frequent the jaw motion artifact was detected in these positions across the cohort. (Note, the 100% size, etc., is indicated outside the figure for reference.) The location of each channel was estimated as the average position (from a two-dimensional projection of our probe) of each channel's source and detector.

changes in concentration, which characterize JM type 1 artifacts [Fig. 3(b)]. This failure is likely related to the poor performance of the algorithm in locating the artifacts. Specifically, the spline algorithm relies on automatically identifying points that are contaminated by motion artifacts. This identification is based on abrupt changes in signal intensity. Since JM promotes consistent abrupt oscillations, the automated detection fails to identify the artifacts, because it starts to treat the oscillations as a reliable feature. Type 1 artifacts are more frequent than type 2; therefore, the performance of the spline algorithm “alone” to correct all trials was very poor. Alone, the spline algorithm properly corrected only 10% of all the trials affected by motion.

Since the performance of wavelet and spline was complementary (the 10% spline success is possibly a subset of the 10% of data that the wavelet could not correct), we hypothesized that the most efficient approach to remove artifacts in speech tasks would be to combine the spline and the wavelet algorithms. To this end, first, the spline algorithm interpolation is used to correct baseline changes, since the wavelet decomposition does not properly handle baseline changes (it can induce data trends). Wavelet decomposition is applied to the data after the spline algorithm is complete. Figure 3(c) shows the effect of our proposed approach in a representative time series around the JM task. Compared to wavelet filtering only, the hybrid procedure has a positive impact on correcting JM artifacts of type 2, since it removes artificial data trends, while it does not yield any negative effect on JM artifacts of type 1. The improvement of performance on type 2 artifacts generates a better rate of corrected trials, i.e., the hybrid approach corrected ~94% of the data across all subjects without creating long-term trends.

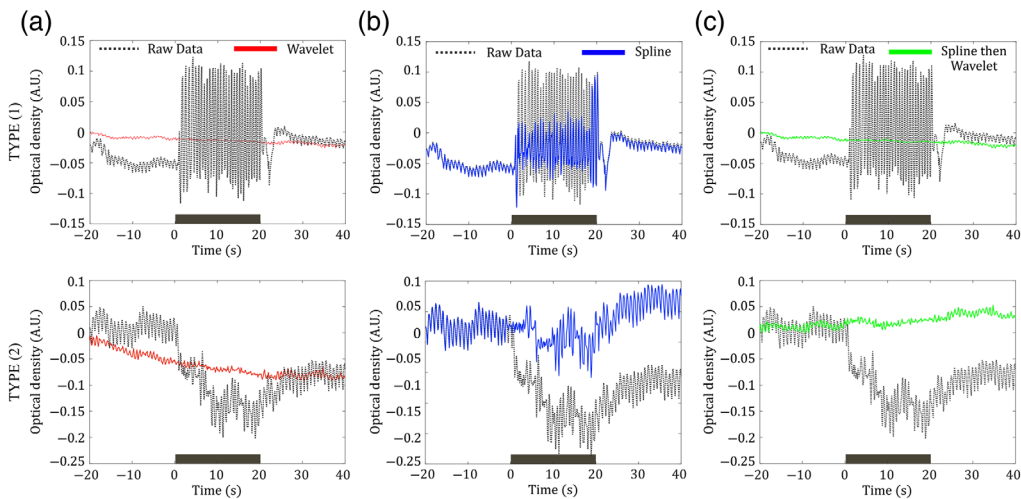


**Fig. 3** Performance of motion artifact removal in decontaminating (“removing/fixing”) JM artifacts in one illustrative subject. Each algorithm was tested separately in both type 1 (top row) and type 2 (bottom row) artifacts. In all plots, the gray line represents the raw optical density (760 nm) time series for a representative channel. Red, blue, and green colors correspond, respectively, to the optical time series after motion correcting with wavelet decomposition, spline interpolation, and the hybrid algorithm (i.e., spline interpolation followed by wavelet decomposition). (a) and (b) The performance of wavelet decomposition and spline interpolation, respectively, on motion artifacts. (c) The performance of our hybrid procedure for correcting motion artifacts.

### 3.3 Validation of the Proposed Algorithm in Reading Tasks

Lastly, we validated our approach in an experimental protocol of healthy subjects during reading tasks. We hypothesized that the method of reading (RA versus SR) should not change the functional activation pattern measured by fNIRS during the task. That is, after JM is factored out, the functional activation responses should be similar for RA and SR. Figure S1 in the [Supplementary Material](#) shows a representative example of how the motion of the anterior temporal muscle affects the optical signal during a RA trial.

Our first observation is that a robust method for correcting motion artifacts saves more data for analysis. Without correcting the motion artifacts during the RA task, for example,  $\sim 76\%$  of the subjects (31/41) would have been discarded because they did not present any channel with characteristic hemodynamic response. This situation changes after correcting for motion artifacts. When applying the wavelet decomposition algorithm only and the hybrid algorithm, respectively, we were able to analyze data from 18 and 23 subjects, respectively, which represent 43% and 56% of the total cohort, respectively.

The group response during RA and SR is shown in Fig. 5 for the three cases considered already (no motion artifact correction, wavelet correction only, and hybrid approach). When motion artifact correction was applied, Broca’s and Wernicke’s areas had a relatively high frequency in both tasks, as is expected for reading tasks. However, the activated regions are more similar between the two reading tasks after correcting motion artifacts with the hybrid approach [Fig. 4(c)]. It is also interesting to note that the motion artifact correction was even important for improving the response of the SR task. This improvement is expected, since JM is not the only source of motion artifact in fNIRS data.

We compared the temporal dynamics of the HRF for both reading tasks after using the hybrid approach for motion artifact correction. Notice the hybrid algorithm provided the highest spatial agreement between the activated regions due to RA and SR (Fig. 5). In all activated ROIs, we observed excellent agreement between the averaged HbO and HbR. The Pearson’s correlation coefficients for the curves obtained during RA versus the curves obtained during SR ranged from 0.53 to 0.96, again demonstrating that the hybrid algorithm provides robust results both in the area of activation and in the dynamics of the response measured. Interestingly, by comparing the average HRF of both tasks it is possible to see that RA and reading silently induces changes with

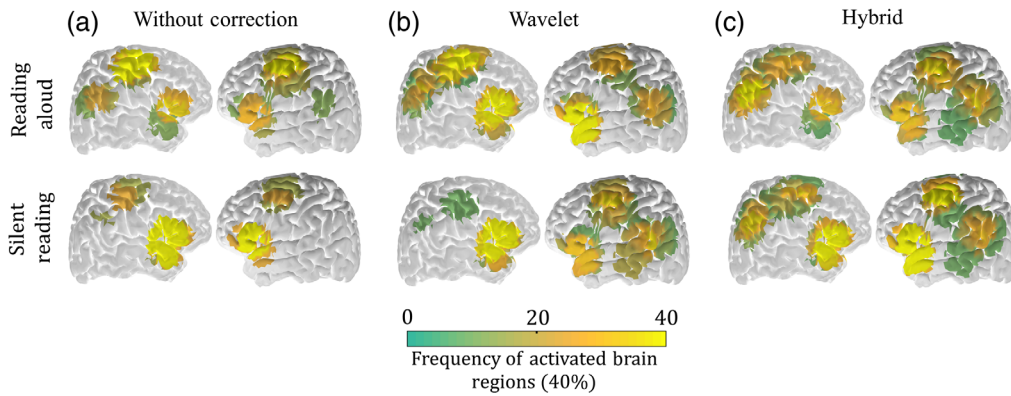


**Fig. 4** Comparison between activated brain regions from RA (first row) and SR (second row) as a function of processing of motion artifacts: (a) without any motion artifact correction, (b) after using wavelet only correction, and (c) after using hybrid procedure to remove motion artifacts. Each brain region is colored based on the frequency of activation across the group, considering only subjects that had at least one activated channel. Channels that presented characteristic hemodynamic response for oxy-hemoglobin (HbO) and deoxy-hemoglobin (HbR) were considered to be activated. From the plots it is possible to notice that the hybrid method yields the closest match between the two tasks, both qualitatively (i.e., the regions activated) and quantitatively (i.e., the frequency of activation of each region). The wavelet-only correction underestimates the activated areas in the parietal regions in both hemispheres.

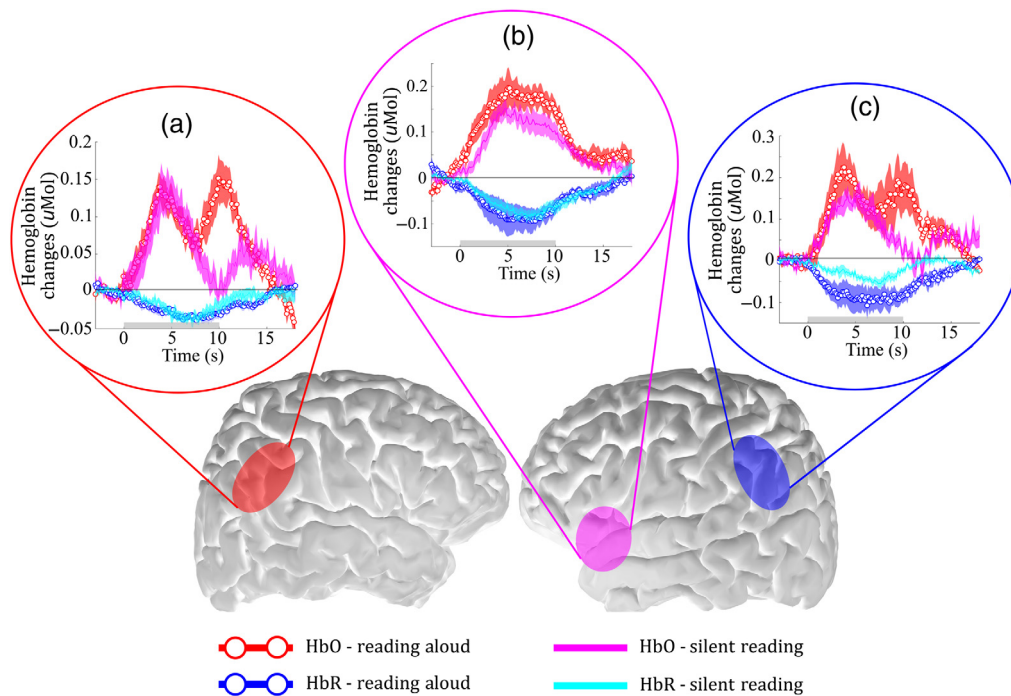


**Fig. 5** Temporal dynamics of the HRF due to reading tasks across all subjects from three different ROIs: (a) posterior region in the right hemisphere (contralateral to Wernicke's), (b) Broca's area, and (c) Wernicke's area (left hemisphere) after applying our hybrid method to remove motion artifact. The gray bar on the plots indicates when the task was performed, and the shaded error bars are the standard error across all channels in the ROI. All ROIs are localized in the brain to facilitate visualization.

similar amplitudes in all ROIs analyzed. Typically, motion artifacts induced by the temporal muscle increase HbO and HbR changes by 10-fold.<sup>57</sup> The similarity in amplitude that we found in the two reading tasks further suggests that the artifacts due to the temporalis muscle were properly corrected with our hybrid algorithm.

## 4 Discussion

Owing to its high portability and ease of use, fNIRS is attractive for measurement of brain activation in functional protocols involving speech.<sup>8,36,37,69</sup> The fNIRS time-series data, however, must be carefully analyzed and interpreted since the technique is sensitive to confounding factors such as motion artifacts and extracortical hemodynamic changes.<sup>38–43,44,45,51,55,68,70–73</sup> Despite recent efforts to standardize fNIRS processing workflow, certain applications of fNIRS may need unique methods to deal with inherent artifacts underlying a specific task and/or experimental protocol. In this work, we aimed to investigate this issue per use of fNIRS in speech-related protocols. We demonstrated a method for data analysis of such functional protocols that is readily standardized.

In many speech-related tasks, the motion of the temporalis muscle (associated with JM) can lead to unique motion artifacts.<sup>56</sup> In this work, we attempted to characterize the artifacts in speech by performing fNIRS measurements during JM. We observed that JM produces two main types of motion artifacts (Fig. 2): abrupt, nonharmonic oscillations specific to voice production (type 1) and baseline changes (type 2). While type 1 artifacts greatly affect most of the channels located in the frontal and temporal lobes, type 2 artifacts were found in more posterior channels and played a major role in long-duration tasks [Fig. 2(c)]. Type 2 artifacts are commonly reported as motion artifacts in any fNIRS study, but type 1 artifacts have been under-reported because previous studies largely used band-pass filtering in fNIRS analysis. The use of low-pass filters smooths out the oscillation pattern but leaves signatures at the same frequencies of the task-induced changes. Importantly, since these artifacts are correlated with the task, they can lead to significant hemoglobin variation during the task, i.e., if not corrected properly.

To properly correct fNIRS data for speech protocols, we demonstrated a hybrid motion artifact removal algorithm by combining two complementary methods: spline interpolation and wavelet decomposition, in this order. This approach has been recently suggested to correct motion artifacts produced in infant fNIRS data,<sup>74</sup> and our work extends its use to another protocol that is also affected by motion. Moreover, the hybrid approach is based on the expectation that spline interpolation can efficiently correct baseline changes (type 2 artifacts) but fails to remove abrupt oscillations due to the motion of the jaw (type 1 artifacts). Wavelet regression alone could remove JM artifacts efficiently, but in practice it created long-term trends and skewed the data [Fig. 3(a)]. This limitation of wavelet correction is in agreement with previous reports.<sup>55,75</sup>

As an aside, we compared the performance of the hybrid method with the correlation-based signal improvement (CBSI) approach,<sup>54</sup> which has been noted as an alternative method for analyzing tasks involving language protocols.<sup>36,53</sup> With our JM data, the hybrid method performed better than the CBSI algorithm (results not shown). CBSI could only fully correct 12 of 41 subjects. More importantly, three subjects had more than 10 uncorrected channels by the CBSI. Both the wavelet-only and the hybrid algorithms had 0 subjects with more than 10 uncorrected channels. This poor performance of the CBSI method in real data is in agreement with previous reports.<sup>53,75</sup> In addition, we believe that our approach is less limited than CBSI, since it does not force anticorrelations between oxyhemoglobin and deoxyhemoglobin concentration changes. Note the opposite behavior between HbO and HbR is not necessarily expected in all functional tasks,<sup>49,76</sup> and even when it occurs it may not occur at the exact same time. The high temporal resolution of NIRS may lead to spurious correlations as well.<sup>77</sup>

Finally, the hybrid approach was successfully validated in a functional protocol involving reading. We chose this task because reading can be performed both silently and out loud. Therefore, we could analyze the influence of speech in the protocol alone by keeping all other cofactors constant. Our results show that both tasks activate the main areas related to reading, including Broca's and Wernicke's regions (Fig. 4), despite high intersubject variation (as expected for cognitive or higher-processing brain function). Figure 5 compares the average HRF from the two reading tasks measured across all subjects in the main activated regions. The robust similarity of the amplitudes and dynamics of the curves in each brain region suggests that contributions of motion artifacts due to speech were removed.

Despite this effort to remove unwanted contributions from extracortical layers and superficial task-evoked artifacts from systemic physiology, our short-channel regression approach has

limitations. First, due to experimental constraints, we limited the number of short separation channels to two. Previous studies provided evidence that the superficial hemodynamics is not homogenous across the different regions of the brain,<sup>60,78</sup> and therefore the improvement obtained by using two short separation channels decreases as the distance between the short and the long channels increases.<sup>79</sup> Unfortunately, most of the studies that report the task-evoked effects of CO<sub>2</sub> in speech were not performed with short separations (i.e., <1 cm);<sup>47,48</sup> therefore, it is not possible to know how much of these CO<sub>2</sub> effects are from the cortex, and we cannot point whether these effects are still present in some of our channels after short-channel regression. Regardless, we acknowledge that the known task-evoked effects of CO<sub>2</sub>, as well as effects from systemic low-frequency oscillations, might not have been completely eliminated. This would affect mainly the channels furthest away from the short-separation channels. Overall, despite these limitations mentioned, the (temporal and spatial) comparison between the two reading tasks strongly suggests that our proposed workflow removes spurious hemodynamic response in speech and decreases the variability of the hemodynamic response measured in speech-related protocols.

## 5 Conclusions

In this work, we characterized the effects of speech production on the fNIRS signal and developed an approach to ameliorate motion artifacts. We performed a JM task in 50 healthy subjects to characterize the motion artifacts induced by speech, and we observed that JM induces two distinct patterns of motion artifacts in the fNIRS signal. To remove unwanted contributions, we validated a hybrid motion-correction algorithm based, sequentially, on spline interpolation and then wavelet filtering. Finally, we validated the hybrid algorithm in 41 healthy subjects during a reading task performed under two different conditions: RA and SR. After applying the hybrid procedure, we observed good agreement between both tasks, both spatially and temporally. Overall, this study demonstrates a standard processing scheme for fNIRS data during speech protocols that decreases spurious responses and intersubject variability due to motion artifacts.

## Disclosures

The authors have no conflicts of interest to declare.

## Acknowledgments

This work was supported by the Misericordia University Faculty Research Grants Program (G.M.T., C.M.T.), the São Paulo Research Foundation (FAPESP) through Proc. 2013/07559-3 (R.C.M.), 2012/02500-8 (R.C.M.), and 2016/22990-0 (S.L.N.) and the U.S. National Institutes of Health through R01-NS060653 (A.G.Y.) and P41-EB015893 (A.G.Y.). The funders had no role in study design, data collection, and analysis, decision to publish, or preparation of the article.

## References

1. M. A. Franceschini et al., “Hemodynamic evoked response of the sensorimotor cortex measured noninvasively with near-infrared optical imaging,” *Psychophysiology* **40**(4), 548–560 (2003).
2. M. N. Kim et al., “Noninvasive measurement of cerebral blood flow and blood oxygenation using near-infrared and diffuse correlation spectroscopies in critically brain-injured adults,” *Neurocrit. Care* **12**(2), 173–180 (2010).
3. R. C. Mesquita and A. G. Yodh, “Diffuse optics: fundamentals and tissue applications,” in *Nano Optics and Atomics: Transport of Light and Matter Waves*, R. Kaiser, D. S. Wiersma, and L. Fallani, Eds., pp. 51–74, IOS Press, Amsterdam (2011).

4. M. Ferrari and V. Quaresima, "A brief review on the history of human functional near-infrared spectroscopy (fNIRS) development and fields of application," *Neuroimage* **63**(2), 921–935 (2012).
5. D. A. Boas et al., "Twenty years of functional near-infrared spectroscopy: introduction for the special issue," *Neuroimage* **85**, 1–5 (2014).
6. M. Strait and M. Scheutz, "What we can and cannot (yet) do with functional near infrared spectroscopy," *Front. Neurosci.* **8**, 117 (2014).
7. R. McKendrick et al., "Using co-variations in the Hb signal to detect visual activation: A near infrared spectroscopic imaging study," *Neuroimage* **47**(2), 473–481 (2009).
8. A. C. Dieler, S. V. Tupak, and A. J. Fallgatter, "Functional near-infrared spectroscopy for the assessment of speech related tasks," *Brain Lang.* **121**(2), 90–109 (2012).
9. M. Tsuji et al., "Cerebral intravascular oxygenation correlates with mean arterial pressure in critically ill premature infants," *Pediatrics* **106**(4), 625–632 (2000).
10. D. W. Brown et al., "Quantitative near infrared spectroscopy measurement of cerebral hemodynamics in newborn piglets," *Pediatr. Res.* **51**(5), 564–570 (2002).
11. M. Dehaes et al., "Perioperative cerebral hemodynamics and oxygen metabolism in neonates with single-ventricle physiology," *Biomed. Opt. Express* **6**(12), 4749–4767 (2015).
12. S. R. de Oliveira et al., "Association between hemodynamic activity and motor performance in six-month-old full-term and preterm infants: a functional near-infrared spectroscopy study," *Neurophotonics* **5**(1), 011016 (2017).
13. S. R. de Oliveira et al., "Changes of functional response in sensorimotor cortex of preterm and full-term infants during the first year: an fNIRS study," *Early Hum. Dev.* **133**(April), 23–28 (2019).
14. P. Farzam et al., "Shedding light on the neonatal brain: probing cerebral hemodynamics by diffuse optical spectroscopic methods," *Sci. Rep.* **7**(1), 15786 (2017).
15. T. P. Beausoleil et al., "Cerebral oxygen saturation and peripheral perfusion in the extremely premature infant with intraventricular and/or pulmonary haemorrhage early in life," *Sci. Rep.* **8**(1), 6511 (2018).
16. H. Watanabe, F. Homae, and G. Taga, "General to specific development of functional activation in the cerebral cortexes of 2- to 3-month-old infants," *Neuroimage* **50**(4), 1536–1544 (2010).
17. E. M. Buckley et al., "Cerebral hemodynamics in preterm infants during positional intervention measured with diffuse correlation spectroscopy and transcranial Doppler ultrasound," *Opt. Express* **17**(15), 12571–12581 (2009).
18. N. Roche-Labarbe et al., "Somatosensory evoked changes in cerebral oxygen consumption measured non-invasively in premature neonates," *Neuroimage* **85**, 279–286 (2014).
19. S. M. Liao et al., "Neonatal hemodynamic response to visual cortex activity: high-density near-infrared spectroscopy study," *J. Biomed. Opt.* **15**(2), 026010 (2010).
20. T. Durduran et al., "Optical measurement of cerebral hemodynamics and oxygen metabolism in neonates with congenital heart defects," *J. Biomed. Opt.* **15**(3), 037004 (2010).
21. N. Roche-Labarbe et al., "Near-infrared spectroscopy assessment of cerebral oxygen metabolism in the developing premature brain," *J. Cereb. Blood Flow Metab.* **32**(3), 481–488 (2012).
22. P.-Y. Lin et al., "Non-invasive optical measurement of cerebral metabolism and hemodynamics in infants," *J. Vis. Exp.* **73**, e4379 (2013).
23. P. Y. Lin et al., "Reduced cerebral blood flow and oxygen metabolism in extremely preterm neonates with low-grade germinal matrix-intraventricular hemorrhage," *Sci. Rep.* **6**(April), 25903 (2016).
24. V. Jain et al., "Cerebral oxygen metabolism in neonates with congenital heart disease quantified by MRI and optics," *J. Cereb. Blood Flow Metab.* **34**(3), 380–388 (2014).
25. M. N. Kim et al., "Continuous optical monitoring of cerebral hemodynamics during head-of-bed manipulation in brain-injured adults," *Neurocrit. Care* **20**(3), 443–453 (2014).
26. O. Steinkellner et al., "Optical bedside monitoring of cerebral perfusion: technological and methodological advances applied in a study on acute ischemic stroke," *J. Biomed. Opt.* **15**(6), 061708 (2010).

27. C. G. Favilla et al., "Optical bedside monitoring of cerebral blood flow in acute ischemic stroke patients during head-of-bed manipulation," *Stroke* **45**(5), 1269–1274 (2014).
28. D. Phillip and H. W. Schyetz, "Spontaneous low frequency oscillations in acute ischemic stroke? A near infrared spectroscopy (NIRS) study," *J. Neurol. Neurophysiol.* **05**(6), 1000241 (2015).
29. L. He et al., "Noninvasive continuous optical monitoring of absolute cerebral blood flow in critically ill adults," *Neurophotonics* **5**(4), 045006 (2018).
30. E. J. Forero et al., "Use of near-infrared spectroscopy to probe occlusion severity in patients diagnosed with carotid atherosclerotic disease," *Med. Res. Arch.* **5**(6), 1–22 (2017).
31. C. Terborg et al., "Bedside assessment of cerebral perfusion reductions in patients with acute ischaemic stroke by near-infrared spectroscopy and indocyanine green," *J. Neurol. Neurosurg. Psychiatr.* **75**(1), 38–42 (2004).
32. S. K. Piper et al., "A wearable multi-channel fNIRS system for brain imaging in freely moving subjects," *Neuroimage* **85**, 64–71 (2014).
33. P. Pinti et al., "A review on the use of wearable functional near-infrared spectroscopy in naturalistic environments," *Jpn. Psychol. Res.* **60**(4), 347–373 (2018).
34. R. McKendrick et al., "Into the wild: neuroergonomic differentiation of hand-held and augmented reality wearable displays during outdoor navigation with functional near infrared spectroscopy," *Front. Hum. Neurosci.* **10**(May), 216 (2016).
35. G. M. Tellis, C. Vitale, and T. Murgallis, "Near infrared spectroscopy (NIRS): a pilot study to measure hemoglobin concentration changes in the brains of persons who stutter and typically fluent speakers," *Procedia—Soc. Behav. Sci.* **193**, 261–265 (2015).
36. B. Walsh et al., "Hemodynamics of speech production: an fNIRS investigation of children who stutter," *Sci. Rep.* **7**(1), 4034 (2017).
37. N. Wan et al., "A functional near-infrared spectroscopic investigation of speech production during reading," *Hum. Brain Mapp.* **39**(3), 1428–1437 (2018).
38. R. Saager and A. Berger, "Measurement of layer-like hemodynamic trends in scalp and cortex: implications for physiological baseline suppression in functional near-infrared spectroscopy," *J. Biomed. Opt.* **13**(3), 034017 (2008).
39. N. M. Gregg et al., "Brain specificity of diffuse optical imaging: improvements from superficial signal regression and tomography," *Front. Neuroenergetics* **2**(1), 1020–1033 (2010).
40. L. Gagnon et al., "Improved recovery of the hemodynamic response in diffuse optical imaging using short optode separations and state-space modeling," *Neuroimage* **56**(3), 1362–1371 (2011).
41. R. C. Mesquita et al., "Influence of probe pressure on the diffuse correlation spectroscopy blood flow signal: extra-cerebral contributions," *Biomed. Opt. Express* **4**(7), 978–994 (2013).
42. J. R. Goodwin, C. R. Gaudet, and A. J. Berger, "Short-channel functional near-infrared spectroscopy regressions improve when source–detector separation is reduced," *Neurophotonics* **1**(1), 015002 (2014).
43. W. B. Baker et al., "Pressure modulation algorithm to separate cerebral hemodynamic signals from extracerebral artifacts," *Neurophotonics* **2**(3), 035004 (2015).
44. S. Brigadoi and R. J. Cooper, "How short is short? Optimum source–detector distance for short-separation channels in functional near-infrared spectroscopy," *Neurophotonics* **2**(2), 025005 (2015).
45. M. A. Yücel et al., "Short separation regression improves statistical significance and better localizes the hemodynamic response obtained by near-infrared spectroscopy for tasks with differing autonomic responses," *Neurophotonics* **2**(3), 035005 (2015).
46. R. B. Saager and A. J. Berger, "Direct characterization and removal of interfering absorption trends in two-layer turbid media," *J. Opt. Soc. Am. A* **22**(9), 1874–1882 (2005).
47. F. Scholkmann et al., "End-tidal CO<sub>2</sub>: an important parameter for a correct interpretation in functional brain studies using speech tasks," *Neuroimage* **66**, 71–79 (2013).
48. F. Scholkmann, M. Wolf, and U. Wolf, "The effect of inner speech on arterial CO<sub>2</sub> and cerebral hemodynamics and oxygenation: a functional NIRS study," *Adv Exp. Med. Biol.* **789**, 81–87 (2013).

49. G. A. Zimeo Morais et al., “Non-neuronal evoked and spontaneous hemodynamic changes in the anterior temporal region of the human head may lead to misinterpretations of functional near-infrared spectroscopy signals,” *Neurophotonics* **5**(1), 011002 (2017).
50. T. J. Huppert et al., “HomER: a review of time-series analysis methods for near-infrared spectroscopy of the brain,” *Appl. Opt.* **48**(10), D280–D298 (2009).
51. F. Scholkmann et al., “How to detect and reduce movement artifacts in near-infrared imaging using moving standard deviation and spline interpolation,” *Physiol. Meas.* **31**(5), 649–662 (2010).
52. R. J. Cooper et al., “A systematic comparison of motion artifact correction techniques for functional near-infrared spectroscopy,” *Front. Neurosci.* **6**(Oct), 147 (2012).
53. S. Brigadoi et al., “Motion artifacts in functional near-infrared spectroscopy: a comparison of motion correction techniques applied to real cognitive data,” *Neuroimage* **85**, 181–191 (2014).
54. X. Cui et al., “Functional near infrared spectroscopy (NIRS) signal improvement based on negative correlation between oxygenated and deoxygenated hemoglobin dynamics,” *Neuroimage* **49**(4), 3039–3046 (2010).
55. B. Molavi and G. A. Dumont, “Wavelet-based motion artifact removal for functional near-infrared spectroscopy,” *Physiol. Meas.* **33**(2), 259–270 (2012).
56. M. Scheckmann et al., “The temporal muscle of the head can cause artifacts in optical imaging studies with functional near-infrared spectroscopy,” *Front. Hum. Neurosci.* **11**(September), 456 (2017).
57. N. Volkening et al., “Characterizing the influence of muscle activity in fNIRS brain activation measurements,” *IFAC-Pap. OnLine* **49**(11), 84–88 (2016).
58. G. H. Klem et al., “The ten twenty electrode system: international federation of societies for electroencephalography and clinical neurophysiology,” *American J. EEG Technol.* **1**(1), 13–19 (1961).
59. C. M. Aasted et al., “Anatomical guidance for functional near-infrared spectroscopy: Atlas viewer tutorial,” *Neurophotonics* **2**(2), 020801 (2015).
60. E. Kirilina et al., “The physiological origin of task-evoked systemic artefacts in functional near infrared spectroscopy,” *Neuroimage* **61**(1), 70–81 (2012).
61. D. Delpy et al., “Estimation of optical pathlength through tissue from direct time of flight measurements,” *Phys. Med. Biol.* **33**(12), 1433–1442 (1988).
62. M. A. Franceschini et al., “Diffuse optical imaging of the whole head,” *J. Biomed. Opt.* **11**(5), 054007 (2006).
63. M. Uga et al., “Optimizing the general linear model for functional near-infrared spectroscopy: an adaptive hemodynamic response function approach,” *Neurophotonics* **1**(1), 015004 (2014).
64. T. J. Huppert, “Commentary on the statistical properties of noise and its implication on general linear models in functional near-infrared spectroscopy,” *Neurophotonics* **3**(1), 010401 (2016).
65. P. Pinti et al., “A novel GLM-based method for the Automatic IDentification of functional Events (AIDE) in fNIRS data recorded in naturalistic environments,” *Neuroimage* **155**, 291–304 (2017).
66. F. Scholkmann et al., “A review on continuous wave functional near-infrared spectroscopy and imaging instrumentation and methodology,” *Neuroimage* **85**, 6–27 (2014).
67. Y. Zhang et al., “Eigenvector-based spatial filtering for reduction of physiological interference in diffuse optical imaging,” *J. Biomed. Opt.* **10**(1), 011014 (2005).
68. S. L. Novi, R. B. M. L. Rodrigues, and R. C. Mesquita, “Resting state connectivity patterns with near-infrared spectroscopy data of the whole head,” *Biomed. Opt. Express* **7**(7), 2524–2537 (2016).
69. N. Nakamichi et al., “Cerebral hemodynamics in speech-related cortical areas: articulation learning involves the inferior frontal gyrus, ventral sensory-motor cortex, and parietal-temporal Sylvian area,” *Front. Neurol.* **9**(Nov), 939 (2018).
70. R. C. Mesquita, M. A. Franceschini, and D. A. Boas, “Resting state functional connectivity of the whole head with near infrared spectroscopy,” *Biomed. Opt. Express* **1**(1), 324–336 (2010).

71. M. Caldwell et al., "Modelling confounding effects from extracerebral contamination and systemic factors on functional near-infrared spectroscopy," *Neuroimage* **143**, 91–105 (2016).
72. M. A. Yücel et al., "Mayer waves reduce the accuracy of estimated hemodynamic response functions in functional near-infrared spectroscopy," *Biomed. Opt. Express* **7**(8), 3078–3088 (2016).
73. A. Aarabi, V. Osharina, and F. Wallois, "Effect of confounding variables on hemodynamic response function estimation using averaging and deconvolution analysis: an event-related NIRS study," *Neuroimage* **155**(February), 25–49 (2017).
74. R. Di Lorenzo et al., "Recommendations for motion correction of infant fNIRS data applicable to data sets acquired with a variety of experimental designs and acquisition systems," *Neuroimage* **200**, 511–527 (2019).
75. F. A. Fishburn et al., "NeuroImage temporal derivative distribution repair (TDDR): a motion correction method for fNIRS," *Neuroimage* **184**, 171–179 (2019).
76. G. R. Wylie et al., "Using co-variations in the Hb signal to detect visual activation: a near infrared spectroscopic imaging study," *Neuroimage* **47**(2), 473–481 (2009).
77. H. Santosa et al., "Characterization and correction of the false-discovery rates in resting state connectivity using functional near-infrared spectroscopy," *J. Biomed. Opt.* **22**(5), 055002 (2017).
78. Y. Tong et al., "Low-frequency oscillations measured in the periphery with near-infrared spectroscopy are strongly correlated with blood oxygen level-dependent functional magnetic resonance imaging signals," *J. Biomed. Opt.* **17**(10), 1060041 (2012).
79. L. Gagnon et al., "Short separation channel location impacts the performance of short channel regression in NIRS," *Neuroimage* **59**(3), 2518–2528 (2012).

**Sergio L. Novi** is PhD candidate of the Institute of Physics at the University of Campinas. He earned his BS degree in physics from the University of Campinas. He has been working with functional near-infrared spectroscopy and has developed novel methods in fNIRS processing analysis.

**Erin Roberts** is an adjunct professor and researcher at Misericordia University, as well as a licensed speech-language pathologist. She has completed various research studies in the field of speech-language pathology, and has presented findings at state, national, and international conferences.

**Danielle Spagnuolo:** Biography is not available.

**Brianna M. Spilsbury** is a graduate student clinician and researcher in the Speech-Language Pathology Department at Misericordia University. She is on the Dean's List and has presented papers at state, national, and international conventions. She completed research and data collection for this study.

**D'manda C. Price** is a graduate student clinician and researcher in the Speech-Language Pathology Department at Misericordia University. She is on the Dean's List and is the founder of the American Sign Language Club. She completed research and data collection for this study. She has presented papers at state, national, and international conventions.

**Cara A. Imbalzano** is a graduate student clinician and researcher in the Speech-Language Pathology Department at Misericordia University. She has presented papers at state, national, and international conventions. She completed research and data collection for this study.

**Edwin Forero** is a PhD candidate of the Institute of Physics at the University of Campinas. He earned his BS degree in physics from the National University of Colombia in Bogotá, and his MSc degree in physics at the University of Campinas. His research focuses on novel methods for fNIRS analysis.

**Arjun G. Yodh** is the James M. Skinner Professor of science and director of the Laboratory for Research on the Structure of Matter at the University of Pennsylvania. His current interests span

fundamental and applied questions in condensed matter physics, medical physics, biophysics, and optical sciences. He has made pioneering contributions establishing and demonstrating use of diffuse optics for tissue monitoring and imaging.

**Glen M. Tellis** is a professor of speech-language pathology and chair at Misericordia University in Dallas, PA. He was a SIG4 steering committee member, ASHA's 2010 convention fluency topic chair, and is a BCFS. He has received external funding for his research, taught courses in stuttering, supervised clinics, presented at national and international conferences, and published articles about stuttering.

**Cari M. Tellis** PhD, CCC/SLP, EMT, EMCI is a full, tenured professor in the Speech-Language Pathology Department at Misericordia University and is a licensed and certified speech-language pathologist. Her areas of specialization include voice rehabilitation and training; laryngeal physiology, muscle anatomy and biochemistry; counseling; motor learning and education, as well as voice and speech science. She has authored and co-authored numerous presentations at international, national, and state conferences and has published in reputable journals.

**Rickson C. Mesquita** is associate professor of physics at the University of Campinas (UNICAMP, São Paulo, Brazil). He leads a group in biomedical optics with interests focused on designing new instrumentation and developing innovative methods for diffuse optics in biological tissue. He has experience in translating diffuse optical techniques for clinical and neuroscience applications.